The Results From The NICMOS Parallel Imaging and Grism Survey

Lin Yan

The Carnegie Observatroies, Pasadena, CA91108, email: lyan@ociw.edu

Abstract. We present the results of a survey which utilizes the NICMOS Camera 3 Parallel grism and imaging observations of random fields. We have identified 33 Hα emission-line galaxies at $0.75 < z < 1.9$. The inferred co-moving number density of these objects is $3.3 \times 10^{-4}\ h_{50}^3$ Mpc^{-3}, very similar to that of the bright Lyman break objects at $z \sim 3$. The mean star formation rate of these galaxies 21 M$_\odot$ yr^{-1} for H$_0$ = 50km/s/Mpc. Using this sample, we derived the Hα luminosity function (LF) at $z = 1.3$. The integrated Hα luminosity density at $z \sim 1.3$ is 1.64×10^{40} h$_{50}$ erg s^{-1} Mpc^{-3}, approximately 14 times greater than the local value reported by Gallego et al. (1995). The volume averaged star formation rate at $z = 1.3 \pm 0.5$ is 0.13 M$_\odot$ yr^{-1} Mpc^{-3} without correction for extinction. The SFR derived at $\sim$ 6500 Å is a factor of 3 higher than that deduced from 2800 Å continua. We believe that this difference is largely due to dust extinction. The implied total extinction at 2800Å is in the range of $2-4$ magnitude. However, the precise determination of the total extinction is sensitive to the model assumptions.

Deep ground-based VRI images of the NICMOS fields have revealed roughly a dozen of extremely red objects (EROs) with R $-$ H > 5 and H brighter than 20.6. The surface density of these objects is around 0.6 per square arcminutes.

1. Introduction

NICMOS parallel observations, taken in parallel with one of the other science instruments on HST, has provided us for the first time a wealth of data at near infrared wavelengths with HST resolution. Small background at wavelengths of 0.8μ and 1.6μ and HST high angular resolution make NICMOS a very efficient instrument in studying the faint galaxy population at high redshifts.

The NICMOS parallel imaging and grism observations were both made with Camera 3 with a field of view $\sim 52'' \times 52''$. The imaging data were taken with broad band filters F110W and F160W at 1.1μ (J band) and 1.6μ (H band). The grism data has a spectral resolution of 200 per pixel and covers wavelength regions from 0.8μ to 1.2μ (G096) and 1.1μ to 1.9μ (G141). We have reduced and analysed the NIC3 parallel imaging data covering $\sim$150 sq. arcminutes and the grism data in G141 grism $\sim$65 sq. arcminutes.

2. Emission-line Galaxies and the Hα Luminosity Function at $z \sim 1.3$ from the NICMOS/HST Grism Parallel Observations

The recent detections of dust enshrouded galaxies at $z > 1$ at sub-millimeter wavelengths (Smail, Ivison & Blain 1997; Hughes et al. 1998; Barger et al. 1998; Lilly et al. 1998) suggest that significant amounts of star formation activity at high redshifts may be obscured. Observations in the rest-frame UV wavelength suffer large uncertainties in extinction corrections. Furthermore, little is known about the properties of normal galaxies in the region between $1 < z < 2$, where neither the 4000Å break nor the Ly continuum break are easily accessible. The near-IR offers one means of accessing both redshift indicators and measures of star formation within this critical redshift range.

We have reduced and analysed the NIC3 parallel grism G141 data, covering $\sim$ 65 sq. arcminutes. The details of the data reduction can be found in McCarthy et al. (1999). We found a total of 33 emission line galaxies over an effective co-moving volume of $10^5\ h_{50}^{-3}$ Mpc^3 for $q_0 = 0.5$. The implied co-moving number density of emission line galaxies in the range $0.75 < z < 1.9$ is $3.3 \times 10^{-4}\ h_{50}^3$ Mpc^{-3}, very similar to that of the bright Lyman break objects at $z \sim 3$. These objects have a median Hα luminosity of 2.7×10^{42} erg sec^{-1}. The most, if not all, of the emission lines detected are either Hα or unresolved blend of Hα+[NII]6583/6548. This identification is mostly based on H-band apparent magnitudes, the emission line equivalent widths and the lack of other detected lines within the G141 bandpass. The median H-band apparent magnitude of $\sim$20.5 (which corresponds to a L* galaxy at $z \sim 1.5$) implies that the possibility of the line being [OII] or Hβ is very small. The redshifts of 6 galaxies in our sample have been confirmed by detection of [OII]3727 emission in the optical spectra using LRIS on the Keck 10m telescope (Teplitz et al. 1999; Malkan et al. 1999). The fraction of AGN contamination in our sample is around 10%; for details, see McCarthy et al. (1999). Figure 1 shows the spectra for a subset of galaxies in our sample.

We compute the Hα luminosity function (LF) based on our sample of emission-line galaxies. We have corrected the incompleteness in the original source catalog using simulations. The final correction is significant only in the faintest luminosity bin and our main result does not sensitively depend on that. All of the detailed results are in Yan et al. (1999). Figure 2 shows our derived Hα LF at $z = 1.3$ and the local Hα LF as measured by Gallego et al. (1995). This plot shows strong evolution in the Hα luminosity density from $z \sim 0$ to $z \sim 1.3$. This is no surprise given the evolution in the ultraviolet luminosity density, but our result provides an independent measure of evolution for Hα emission alone. The LF is well fit by a Schechter function over the range $6 \times 10^{41} < \mathrm{L}(H\alpha) < 2 \times 10^{43}$ erg sec^{-1} with L$^* = 7 \times 10^{42}$ erg sec^{-1} and $\phi^* = 1.7 \times 10^{-3}$ Mpc^{-3} for H$_0$ = 50 km s^{-1} Mpc^{-1} and q$_0$ = 0.5. The integrated Hα luminosity density at $z \sim 1.3$ (our median z) is 1.64×10^{40} h$_{50}$ erg s^{-1} Mpc^{-3}, $\sim$14 times greater than the local value reported by Gallego et al. (1995).

We converted the integrated Hα luminosity density to a star formation rate (SFR) using the relation from Kennicutt (1999): SFR(M$_\odot$yr^{-1}) = 7.9×10^{-42}L(Hα)(erg s^{-1}). This assumes Case B recombination at $T_e = 10^4$ K and a Salpeter IMF ($0.1 - 100\ M_\odot$). This conversion factor is about 10% smaller than the value listed in Kennicutt (1983), the difference reflecting updated evo-

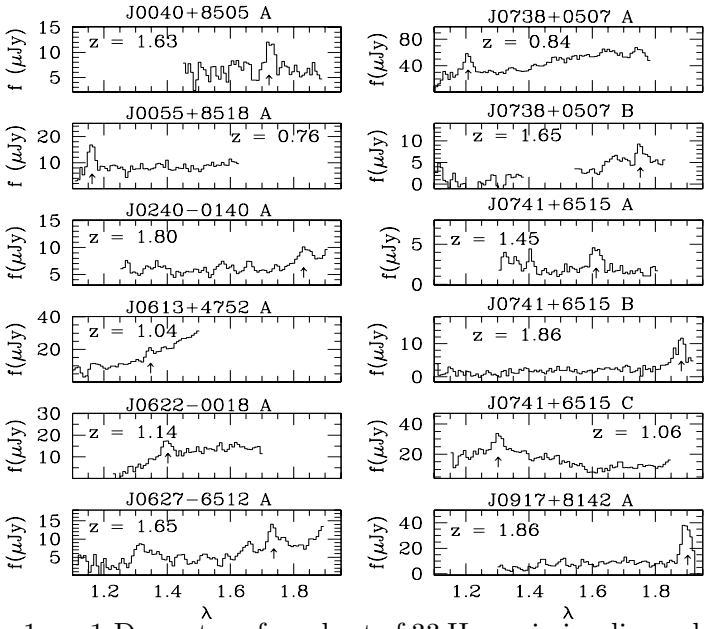

Figure 1. 1-D spectra of a subset of 33 Hα emission-line galaxies. For each object we have marked our candidate emission-lines with arrows below the line. We plot the entire range of the G141 grism for each spectrum even though parts of the spectrum have fallen beyond the field of view of the detector for several objects. The redshifts, assuming an Hα identification for the line are given for each object.

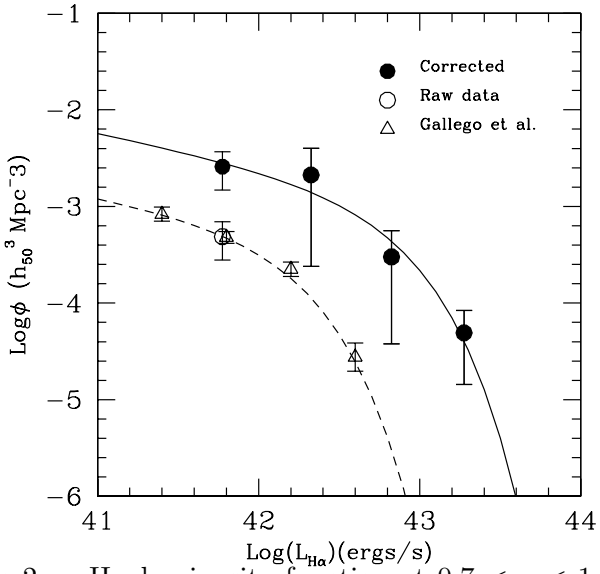

Figure 2. Hα luminosity function at $0.7 < z < 1.9$. The open and filled circles are the data points from our measurements. The open circles represent the raw data and the filled circles are the points corrected for incompleteness. The incompleteness correction is only significant at the faintest luminosity bin. The open triangles show the local Hα luminosity function by Gallego et al. (1995). The solid and dashed lines are the best fits to the data at $z \sim 1.3$ and $z \sim 0$ respectively.

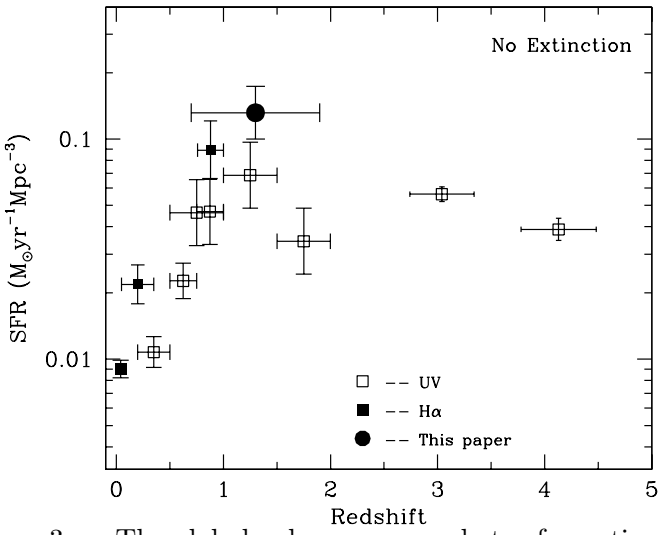

Figure 3. The global volume-averaged star formation rate as a function of redshift without any dust extinction correction. The open squares represent measurements of the 2800Å or 1500Å continuum luminosity density by Lilly et al. (1996), Connolly et al. (1997) and Steidel et al. (1998), whereas the filled squares are the measurements using Hα 6563Å by Gallego et al. (1995), Tresse & Maddox (1996) and Glazebrook et al. (1998). Our result is shown in the filled circle.

lutionary tracks. While different choices of stellar tracks introduce modest uncertainties in the conversion of UV and Hα luminosities to star formation rates, the choice of different IMFs lead to rather large differences. To make consistent comparisons between our results and those in the literature derived from 1500Å and 2800Å UV continuum luminosity densities, we adopt the relation from Kennicutt (1999): $\mathrm{SFR}(\mathrm{M}_\odot\mathrm{yr}^{-1}) = 1.4\times10^{-28}\mathrm{L}(1500-2800\text{Å})(\mathrm{erg\ s^{-1}Hz^{-1}})$. This relation is appropriate for the Salpeter IMF used to derive the Hα conversion factor.

In Figure 3, we plot uncorrected published measurements of the volume-averaged global star formation rate at various epochs. Our result is shown as a filled circle. The star formation rates shown in Figure 3 are calculated from the luminosity densities integrated over the entire luminosity functions, for both Hα and the UV continuum. Lilly et al. and Connolly et al. assumed a faint end slope of -1.3 for the UV continuum luminosity functions at $z \leq 1$. The 1500Å continuum luminosity function at $z \sim 3-4$ measured from Lyman break galaxies by Steidel et al. (1998) has a faint end slope of -1.6.

The clear trend for the longer wavelength determinations of the star formation rate to exceed those based on UV continua is one of the pieces of evidence for significant extinction at intermediate and high redshifts. The amplitude of the extinction correction is quite uncertain Our measurement spans $0.7 < z < 1.9$, overlapping with the Connolly et al. photometric redshift sample and allowing a direct comparison between the observed 2800Å luminosity density and that inferred from Hα. Our Hα-based star formation rate is three times larger than the average of the three redshift bins measured by Connolly et al. (1997).

The star formation rates derived from line or continuum luminosities depend strongly on the choice of IMF, evolutionary tracks, and stellar atmospheres that are input into a specific spectral evolution model. The relevant issue for the present discussion is the ratio of the star formation rates derived from Hα and the 2800Å continuum. This ratio differs significantly for the Scalo and Salpeter IMFs and is a function of metallicity (Glazebrook et al. 1998). Our choice of the Salpeter IMF comes close to minimizing the difference between the published UV- and our Hα-derived star formation rates. The use of a Scalo IMF and solar metallicity would increase the apparent discrepancy by a factor of ~ 2. The only model considered by Glazebrook et al. that further reduces the Hα/2800Å star formation ratio is the Salpeter IMF with the Gunn & Stryker (1983) spectral energy distributions, and this model still leaves us with a factor of ~ 2 enhancement in apparent star formation activity measured at Hα.

If we attribute the entire difference to reddening, the total extinction corrections at 2800Å and Hα are large and model-dependent. The calculation is sensitive to the relative geometry of the stars, gas and dust, as well as the adopted reddening curve. In the extreme case of a homogeneous foreground screen and a MW or LMC reddening curve, we derive $A_{2800} = 2.1$ magnitudes. In local starburst galaxies, differential extinction between the nebular gas, and stellar continuum, and scattering produce an effective reddening curve that is significantly grayer than the MW or LMC curves (Calzetti, Kinney & Storchi-Bergmann 1994; 1996; Calzetti 1997). The Calzetti reddening law (Calzetti 1997) is appropriate for geometries in which the stars, gas and dust are well mixed. In this model, our estimate of the dust extinction at 2800Å is one to two magnitudes larger than in the simple screen case, and is an uncomfortably large correction compared to results from other methods.

3. Extremely Red Objects (EROs)

Several groups have discovered a population of galaxies with extremely red colors R$-$K > 5 or 6. However, the statistics of EROs is still very poor and the nature of these objects remains unclear. The central issue is to understand whether EROs are intrinsically red stellar systems formed at high redshifts in a monolithic collapse or highly reddened starburst galaxies at low to moderate redshifts. The detection of strong sub-mm continuum from ERO HR 10 (Dey et al. 1999; Cimmati et al. 1998) provides conclusive evidence that some of EROs, if not all, are indeed dusty, starburst galaxies at a star formation rate of $500 - 1000 M_\odot$ yr^{-1} at moderate redshifts ($z \sim 1 - 2$).

We have obtained deep ground-based optical images of 27 NIC3 fields, yielding ~ 20 square arcminutes. Among these fields, we have identified about a dozen of EROs with R$-$H > 5 and H brighter than 20.6. The surface density of EROs with H < 20.6 and R$-$H > 5 is roughly 0.6/sq. arcminutes. We also found some evidence that EROs are highly clustered. Among 27 NIC3 fields, we found 2 clusters of EROs. Figure 4 shows a cluster of EROs in a single NIC3 field ($0.75''$) where we also have K-band magnitudes.

Acknowledgments. We thank the staff of the Space Telescope Science Institute for their efforts in making this parallel program possible. This research

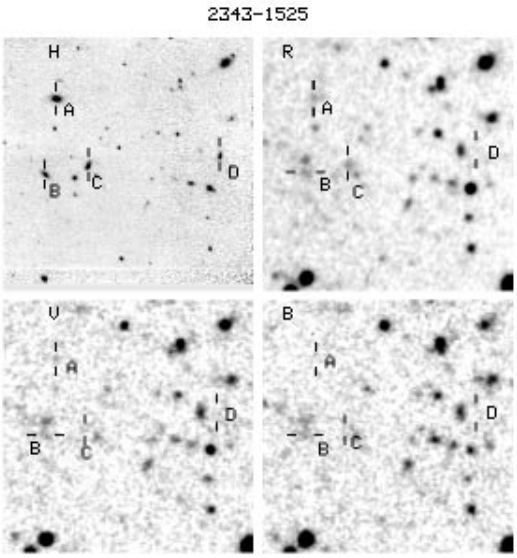

Figure 4. This plot shows a cluster of EROs with BVRH images in a single NIC3 fields (0.75″). All the four EROs have R−K > 6 and the brightest two A and D have K ∼ 18. The deep BVR images were taken with the BTC at CTIO.

was supported, in part, by grants from the Space Telescope Science Institute, GO-7498.01-96A and P423101.

References

Barger, A.J., Cowie, L.L., Sanders, D.B., et al. 1998, Nature, 394, 248
Connolly, A., Szalay, A. S., Dickinson, M., et al. 1997, ApJ, 487, L13
Calzetti, D., Kinney, A.L. & Storchi-Bergmann, T. 1994, ApJ, 429, 582
Calzetti, D. 1997, AJ, 113, 162
Gallego, J., Zamorano, J., Aragon-Salamanca, A., Rego, M. 1995, ApJL, 459, 1
Glazebrook, K., Blake, C., Economou, F., Lilly, S. et al. 1998, astro-ph/9808276
Hughes, D., et al. 1998, Nature, 394, 241.
Kennicutt, R.C. 1999, ARAA, in press. astro-ph/9807187
Kennicutt, R.C. 1983, ApJ, 272, 54
Lilly, S.J., Le Fevre, O., Hammer, F. & Crampton, D. 1996, ApJ, 460, L1
Lilly, S.J., Eales, S.A., et al. 1999, ApJ, in press. astro-ph/9901047
McCarthy, P., Yan, L., 1999, ApJ, august issue, in press, astro-ph/9902347
Steidel C., Dickinson, M., et al. 1998, ApJ, in press. astro-ph/9811399
Teplitz, H., et al. 1999, in prep.
Tresse, L., Maddox, S. 1998, ApJ, 495, 691
Yan, L. McCarthy, P., 1999, ApJ, July issue, in press, astro-ph/9904427